


## Path-orbital-angular-momentum high-dimensional hyperentangled photons from a warm atomic ensemble

Qiwu Hu,<sup>1</sup> Yuan Ren,<sup>1</sup> Xutong Wang <sup>1</sup>, Xiao-Min Hu,<sup>2,3</sup> and Jietai Jing <sup>1,4,5,6,\*</sup>

<sup>1</sup>State Key Laboratory of Precision Spectroscopy, Joint Institute of Advanced Science and Technology, School of Physics and Electronic Science, East China Normal University, Shanghai 200062, China

<sup>2</sup>CAS Key Laboratory of Quantum Information, University of Science and Technology of China, Hefei 230026, China

<sup>3</sup>CAS Center For Excellence in Quantum Information and Quantum Physics, University of Science and Technology of China, Hefei 230026, China

<sup>4</sup>CAS Center for Excellence in Ultra-Intense Laser Science, Shanghai 201800, China

<sup>5</sup>Collaborative Innovation Center of Extreme Optics, Shanxi University, Taiyuan, Shanxi 030006, China

<sup>6</sup>Department of Physics, Zhejiang University, Hangzhou 310027, China



(Received 27 January 2022; accepted 27 May 2022; published 13 June 2022)

We experimentally demonstrate a scheme for the preparation of high-dimensional hyperentangled photon pairs with path degree of freedom (DOF) and orbital-angular-momentum (OAM) DOF using beam displacer (BD) interferometers from a warm atomic ensemble. A strong Gaussian pump beam of fixed frequency passes through the BD to produce a superposition state of two paths. The biphoton state is generated from two parallel spontaneous four-wave mixing processes in the <sup>85</sup>Rb vapor cell. We successfully detect the path entanglement, two-dimensional OAM entanglement, and three-dimensional OAM entanglement by selecting the appropriate measurement. Due to the advantages of the simplicity of our interaction system and high dimensionality of the narrowband hyperentangled photons we generated, such hyperentangled source from an atomic ensemble can be utilized to realize high-dimensional multiple-DOF quantum memory and quantum communication in the future.

DOI: [10.1103/PhysRevA.105.062422](https://doi.org/10.1103/PhysRevA.105.062422)

### I. INTRODUCTION

Quantum entanglement is one of the essential resources for quantum information [1]. Entanglement based on a single degree of freedom (DOF) such as path [2–5], polarization [6,7], frequency [8], photon number [9], and orbital angular momentum (OAM) [10–12] has been extensively studied. Among them, path and OAM have the advantages of high dimensionality [13,14], easy integration [15], and easy implementation of the unitary operation [5]. Hyperentanglement [16–18], consisting of two or more DOFs, has great potential to largely improve the channel capacity of quantum communication and is attracting more and more attention.

The generated entangled photons from widely used nonlinear crystal [6,19] have the characteristic of wide bandwidth ( $\approx$ THz), leading to short coherence time [1]. Another promising way to generate entangled photons is to exploit the spontaneous four-wave mixing (SFWM) process in the atomic ensemble [7]. Generation of narrowband biphotons has been realized in both cold and warm atom ensembles [20–22]. Recently, subnatural-linewidth ( $< 6$  MHz) biphotons [23], time-energy entanglement [24], and polarization entanglement using Sagnac interferometers [7] from warm atomic ensembles have been reported. OAM, one of the fundamental photonic spatial properties, provides a discrete and unbounded state space. It is a promising platform to test the foundations of quantum physics and has great potential of carrying enormous quantum information [10,14]. Up to now, based on hot atomic

ensembles, many achievements related to OAM in the discrete variable (DV) region have been reported, such as OAM entangled photon pairs [25] and qutrits [26]. In the continuous variable (CV) region, there are also some recent progresses, such as OAM multiplexed bipartite entanglement [27], multipartite entanglement [28–30], and deterministic all-optical quantum teleportation [31].

In this paper, we report the experimental generation of path-OAM hyperentanglement with beam displacer (BD) interferometers [32] in a Doppler-broadened warm atomic ensemble, which is inspired by the idea of illuminating two separate regions of a nonlinear medium to produce entangled photons [33]. The generated signal (or idler) photons from two parallel SFWM processes are merged into one path via the BD, which ensures the long-term stability of the generated state. By switching the flip mirrors (Flips), we detect both path entanglement and two-dimensional OAM entanglement, and even three-dimensional OAM entanglement. This is a constructive step to create path-OAM high-dimensional DV hyperentanglement from this double- $\Lambda$  configuration system in a quantum information study. Since the double- $\Lambda$  configuration used in our scheme has found many applications in the CV region [27–30,34–36], our results here pave the way for exploring DV-CV hybrid quantum systems [37–39] from a warm atomic ensemble.

### II. EXPERIMENTAL REALIZATION

The experimental setup is sketched in Fig. 1(a). A Gaussian laser beam with a frequency of 377 110 GHz is produced by a

\*Corresponding author: [jtjing@phy.ecnu.edu.cn](mailto:jtjing@phy.ecnu.edu.cn)

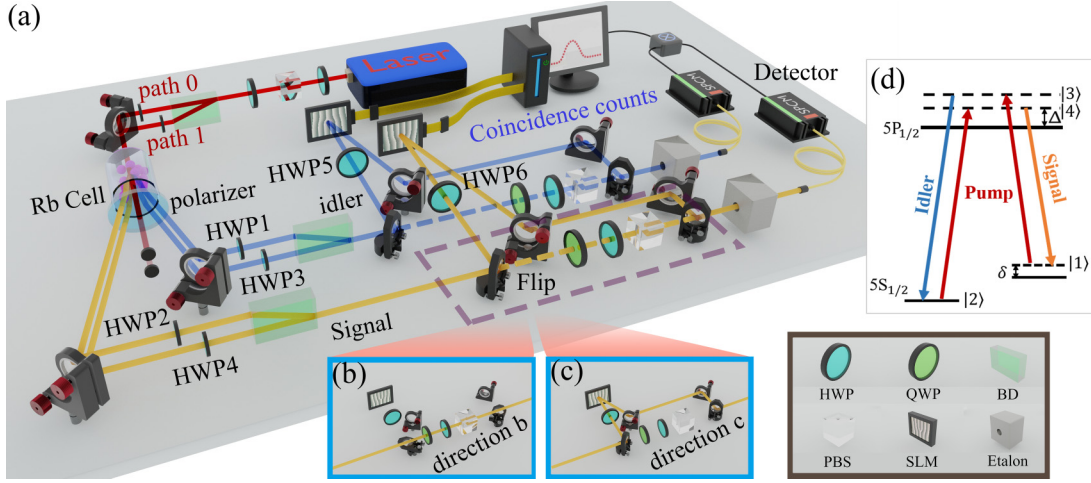


FIG. 1. Schematic for path-OAM high-dimensional hyperentanglement. (a) The experimental setup, including half-wave plate (HWP), quarter-wave plate (QWP), beam displacer (BD), polarization beam splitter (PBS), folding mirror (Flip), spatial light modulator (SLM), and temperature-controlled etalon (Etalon). (b) Direction b for measuring path entanglement. (c) Direction c for measuring OAM entanglement. (d) Double- $\Lambda$  energy-level diagram of  $^{85}\text{Rb}$  in SFWM.  $\Delta$  one-photon detuning.  $\delta$  two-photon detuning.

semiconductor laser. Two half-wave plates (HWPs) and a polarized beam splitter (PBS) are used to control its intensity and polarization conveniently. By setting up the BD [32] appropriately, two pump beams are prepared in two separate paths, and the distance between them is about 4 mm. We obtain the initial state of the path coding  $|\varphi\rangle_0 = 1/\sqrt{2}(|0\rangle_p + |1\rangle_p)$ , where  $p$  denotes the path DOF, and  $|0\rangle_p$  and  $|1\rangle_p$  correspond to the top path and the bottom path created by the BD, respectively. After that, we put two small HWPs after the BD to convert the polarization of pump photons to vertical polarization. Then the two beams with power of about 800 mW are injected into a single warm  $^{85}\text{Rb}$  cell, where two parallel SFWMs occur. The  $^{85}\text{Rb}$  cell is 12 mm long and its temperature is stabilized at  $70^\circ\text{C}$ . The waist diameters of pump beams are both set to  $700\ \mu\text{m}$  at the center of the  $^{85}\text{Rb}$  cell. A double- $\Lambda$  energy-level diagram of  $^{85}\text{Rb}$  is shown in Fig. 1(d). The phase-matched signal and idler photons are emitted at an angle of 7 mrad on both sides of the pump beam. The biphoton state of path 0 after SFWM evolves into

$$|\varphi\rangle_{\text{SFWM}_0} = |0\rangle_{s,p}|0\rangle_{i,p} = |0\rangle_p|0\rangle_p, \quad (1)$$

where  $s$  and  $i$  correspond to the signal and idler photons. Similarly, SFWM in path 1 produces the biphoton in the state of  $|\varphi\rangle_{\text{SFWM}_1} = |1\rangle_p|1\rangle_p$ . In order to select horizontal polarization of the generated photons and suppress the residual pump beam, we put a polarizer behind the  $^{85}\text{Rb}$  cell. The entangled state of the path can be written as

$$|\varphi\rangle_p = \frac{1}{\sqrt{2}}(|0\rangle_p|0\rangle_p + |1\rangle_p|1\rangle_p). \quad (2)$$

The polarization of the generated photons for each path can be changed by putting in two small HWPs for later detection of path information. By rotating HWP1 and HWP2 appropriately, the polarization of generated signal and idler photons in path 0 can be changed to vertical polarization. Similarly, the polarization of the photons in path 1 are set to be horizontal by rotating HWP3 and HWP4.

All of the signal and idler photons produced in our setup are in Laguerre-Gaussian ( $\text{LG}_l$ ) states, where  $l$  denotes the topological charge of the OAM state. OAM conservation [40] ensures that if the state of the signal photon is  $|l\rangle$ , the state of the corresponding idler photon will be  $| -l\rangle$ . The OAM entangled state in our system can be expressed as

$$|\varphi\rangle_l = \sum_{l=-\infty}^{l=\infty} \alpha_l |l\rangle \otimes | -l\rangle, \quad (3)$$

where  $\alpha_l$  denotes the normalization coefficient. Here we study the OAM states carrying topological charges of  $l = 1$  and  $-1$ , which can be denoted by  $|1_l\rangle$  and  $| -1_l\rangle$ . Hence two-dimensional OAM entanglement can be written as

$$\begin{aligned} |\varphi\rangle_{\text{OAM}} &= \alpha_1 |1_l\rangle_s | -1_l\rangle_i + \alpha_{-1} | -1_l\rangle_s |1_l\rangle_i \\ &= \alpha_1 |1_l\rangle_l | -1_l\rangle_l + \alpha_{-1} | -1_l\rangle_l |1_l\rangle_l. \end{aligned} \quad (4)$$

Combining Eqs. (2) and (4), we can get the biphoton hyperentangled state:

$$\begin{aligned} |\psi\rangle &= \frac{1}{\sqrt{2}}(|0\rangle_p|0\rangle_p + |1\rangle_p|1\rangle_p) \\ &\otimes (\alpha_1 |1_l\rangle_l | -1_l\rangle_l + \alpha_{-1} | -1_l\rangle_l |1_l\rangle_l). \end{aligned} \quad (5)$$

In other words, we can manage to obtain the path-OAM two-dimensional hyperentangled state from two parallel SFWMs with BD interferometers.

### III. MEASUREMENTS AND RESULTS

#### A. Tomography of path-OAM hyperentanglement

To read out the hyperentangled information contained in the generated photons, we select the appropriate measurements. As shown in Fig. 1(a), we put four Flips on the paths to lead the beams to travel along direction b or direction c which correspond to the measurement of path or OAM entanglement, respectively. In this way, we can detect the entanglement of each DOF separately. When the Flips are

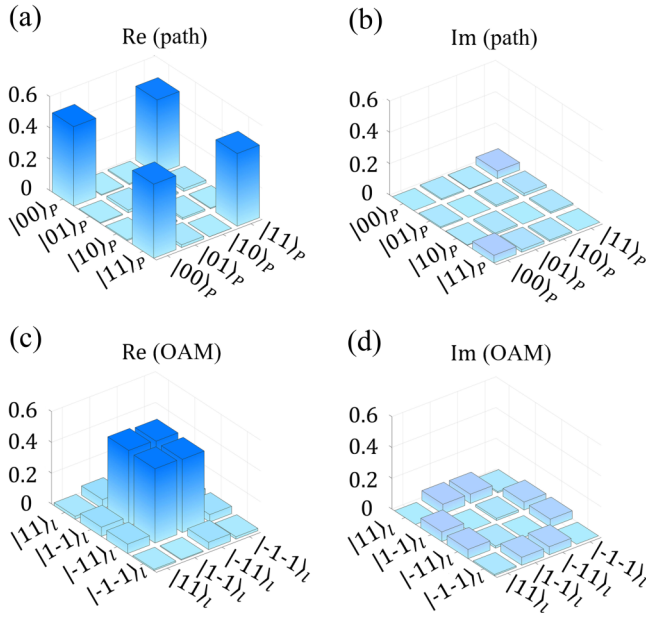


FIG. 2. Results of quantum state tomography of path-OAM hyperentanglement. (a), (b) Real and imaginary parts of path entanglement, respectively. (c), (d) Real and imaginary parts of two-dimensional OAM entanglement, respectively.

folded down as shown in Fig. 1(b), signal and idler photons travel along their respective direction  $b$  to the apparatus of quantum state tomography of the path state [41]. Each apparatus is made up of a HWP, a quarter-wave plate (QWP), and a PBS.

Before the photons are collected by the single-mode fibers, they have to pass through the homemade temperature-controlled etalons. Each etalon has a linewidth of  $\approx 100$  MHz, and its temperature can be controlled from 15 to 25 °C for selecting signal and idler photons. The signal (idler) photon is redshifted (blueshifted) by 3.20 GHz from the pump photon. These etalons largely suppress the unrelated photons from pump scattering. Finally, the photons are detected by the single-photon counting modules. Under the current experimental condition, the total photon collection efficiency is about 10%, and the maximal photon rates for signal and idler channels of our source are 75.2 and 68.8 kHz, respectively. The corresponding linewidth is about 286 MHz. The Cauchy-Schwarz inequality (CSI)  $[g_{s,i}^{(2)}(0)]^2/[g_{s,s}^{(2)}(0)g_{i,i}^{(2)}(0)] \leq 1$  is violated by more than four standard deviations. Such violation is a binary test in the sense that violation of the CSI indicates the presence of nonclassical correlations, which means the system can only be quantum in nature. In order to obtain the density matrix of path entanglement, the coincidence counts are obtained from four sets of orthogonal projection measurement bases on each path, i.e.,  $|0\rangle_p$ ,  $|1\rangle_p$ ,  $|+\rangle_p = \frac{1}{\sqrt{2}}(|0\rangle_p + |1\rangle_p)$ , and  $|i\rangle_p = \frac{1}{\sqrt{2}}(|0\rangle_p + i|1\rangle_p)$ . The density matrix is reconstructed and shown in Figs. 2(a) and 2(b). As we can see, this is the maximally entangled state of combination of  $|00\rangle_p$  and  $|11\rangle_p$ . The bipartite entanglement can be quantified with the concurrence [defined as  $\max\{0, \sqrt{\lambda_1} - \sqrt{\lambda_2} - \sqrt{\lambda_3} - \sqrt{\lambda_4}\}$ , where  $\lambda_i$  are the positive eigenvalues of the matrix

$\rho(\sigma_y \otimes \sigma_y)\rho^*(\sigma_y \otimes \sigma_y)$  in decreasing order and  $\sigma_y$  is the Pauli matrix] [41] and concurrence = 1 corresponds to a maximally entangled state. Based on our measurement results, the purity ( $\text{tr}[\rho^2]$ ) of the state is  $0.929 \pm 0.013$  and its concurrence is  $0.929 \pm 0.010$ , confirming the path entanglement of the photon pair. Another way to certify the entanglement of the quantum state is to utilize the Clauser-Horne-Shimony-Holt type of Bell inequality [42]. On the basis of local realism, the Bell parameter  $S$  of the Bell inequality must obey  $S \leq 2$ . The measured Bell parameter  $S$  for the above path entanglement is  $2.651 \pm 0.039$ , violating the Bell inequality and confirming the existence of path entanglement.

For measuring the entanglement of the OAM DOF, signal (idler) photons propagate directly to HWP6 (HWP5) and the computer-controlled spatial light modulator (SLM) along their respective direction  $c$  when the Flips are folded up as shown in Fig. 1(c). Here we set HWP5 and HWP6 at 22.5° to ensure the horizontal polarized photons modulated by SLM come from path 0 and path 1. By loading the hologram of  $l = 1$  onto the SLM, the generated photon carrying topological charge  $l = -1$  can convert to Gaussian mode and then enter the single-mode fiber. The measurement bases are defined as  $|1\rangle_l$ ,  $|-1\rangle_l$ ,  $|+\rangle_l = \frac{1}{\sqrt{2}}(|1\rangle_l + |-1\rangle_l)$ , and  $|i\rangle_l = \frac{1}{\sqrt{2}}(|1\rangle_l + i|-1\rangle_l)$ . The coincidence counts are acquired and the corresponding results of the density matrix are shown in Figs. 2(c) and 2(d). Based on these results, the purity of the state is  $0.982 \pm 0.017$ , the concurrence is  $0.931 \pm 0.012$ , and the measured Bell parameter  $S$  of the two-dimensional OAM state is  $2.683 \pm 0.049$ , indicating the existence of two-dimensional OAM entanglement. Therefore, we have successfully detected both path entanglement and two-dimensional OAM entanglement, confirming the existence of path-OAM hyperentanglement.

## B. Violation of high-dimensional Bell inequalities

Moreover, we have a further study in demonstrating OAM entanglement in higher dimensions [13,14], which can carry more quantum information and thus play a significant role in quantum communication. By preparing the OAM holograms of  $l = 0, 1$ , and  $-1$  followed by the theory of generalized Bell inequalities for arbitrarily high-dimensional systems proposed by Collins *et al.* [43], the three-dimensional OAM entangled state can be detected. The path-OAM high-dimensional hyperentangled state can be expressed as

$$|\phi\rangle = \frac{1}{\sqrt{2}}(|0\rangle_p|0\rangle_l + |1\rangle_p|1\rangle_l) \otimes (\alpha_0|0\rangle_l|0\rangle_l + \alpha_1|1\rangle_l|-1\rangle_l + \alpha_{-1}|-1\rangle_l|1\rangle_l). \quad (6)$$

Different from previous measurements, we use a relatively convenient method to detect three-dimensional OAM entanglement [14]. Reading out the entanglement of two  $d$ -dimensional systems requires two observers, Alice and Bob, on their respective subsystems, which correspond to signal and idler photons from SFWMs. The measurement bases of signal and idler photons are defined

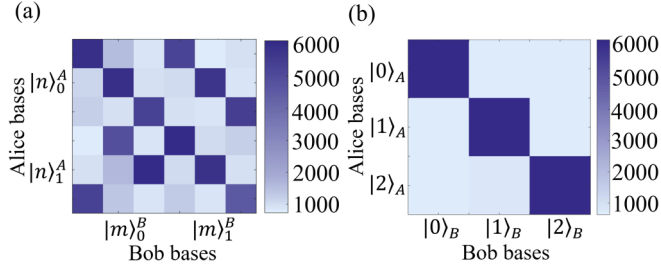


FIG. 3. The measured results of three-dimensional OAM entanglement. (a) The correlation matrix shows the measured coincidence counts in the Bell measurement bases  $|n\rangle_a^A$  and  $|m\rangle_b^B$ . (b) The correlation matrix shows the coincidence counts in the MUB  $|w\rangle$ .

as

$$|n\rangle_a^A = \frac{1}{\sqrt{d}} \sum_{j=0}^{d-1} \exp\left[i\frac{2\pi}{d}j(n + \alpha_a)\right] |j\rangle_A, \quad (7)$$

$$|m\rangle_b^B = \frac{1}{\sqrt{d}} \sum_{j=0}^{d-1} \exp\left[i\frac{2\pi}{d}j(-m + \beta_b)\right] |j\rangle_B, \quad (8)$$

where  $a \in \{0, 1\}$ ,  $b \in \{0, 1\}$ ,  $\alpha_0 = 0$ ,  $\alpha_1 = 1/2$ ,  $\beta_0 = 1/4$ , and  $\beta_1 = -1/4$  while  $n$  and  $m$  both run from 0 to  $d - 1$ , where we set  $d = 3$ .

When the photons are selected to travel along direction  $c$ , SLMs load holograms according to Eqs. (7) and (8). The measured results detected by 36 measurement bases are shown in Fig. 3(a). The expression for the generalized Bell parameter can be written as

$$S_d = \sum_{k=0}^{\lfloor d/2 \rfloor - 1} \left(1 - \frac{2k}{d-1}\right) \{ [P(A_0 = B_0 + k) + P(B_0 = A_1 + k + 1) + P(A_1 = B_1 + k) + P(B_1 = A_0 + k)] - [P(A_0 = B_0 - k - 1) + P(B_0 = A_1 - k) + P(A_1 = B_1 - k - 1) + P(B_1 = A_0 - k - 1)] \}, \quad (9)$$

where  $S_d(\text{local realism}) \leq 2$ , for  $d \geq 2$ .  $P(A_a = B_b + k)$  is the probability that the outcome  $B_b$  differs from  $A_a$  by  $k$ , modulo  $d$ ; it is expressed as

$$P(A_a = B_b + k) = \sum_{j=0}^{d-1} P[A_a = j, B_b = (j + k) \bmod d]. \quad (10)$$

Similarly,

$$P(B_b = A_a + k) = \sum_{j=0}^{d-1} P[B_b = j, A_a = (j + k) \bmod d]. \quad (11)$$

From Eqs. (9)–(11), we can obtain the  $S_d$  value of the three-dimensional OAM state. Based on our measurement, the corresponding Bell-type parameter  $S_3$  is  $2.339 \pm 0.038$ , which violates the limit of local realism  $S_d \leq 2$  and thus is sufficient to verify the quantum nonlocality of the three-dimensional system in our experiment. The experimental violation of the Bell inequality of path entanglement, two-dimensional OAM,

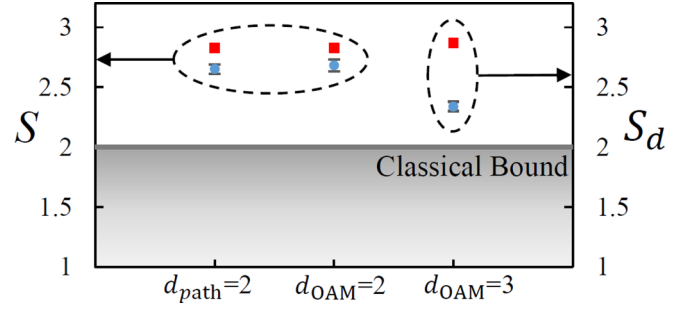


FIG. 4. Violation of high-dimensional Bell inequality. The blue (circular) points represent the experimental values of path, two-dimensional OAM, and three-dimensional OAM in sequence, and experimental errors are derived from the Poisson statistic. The red (block) points represent the theoretical values obtained for the maximally entangled states.

and three-dimensional OAM entanglement are plotted as the blue circular points in Fig. 4. It is clear that they are all higher than the classical bound of 2 (plotted by the gray line). The corresponding theoretical values are shown as the red block points.

Additionally, based on the theory proposed by Bavaresco *et al.* [44], we can acquire the fidelity of high-dimensional entanglement through measurements in mutually unbiased basis (MUB)  $|w\rangle$  [45], which can be constructed from the LG bases  $|j\rangle$ :

$$|w\rangle = \frac{1}{\sqrt{d}} \sum_{j=0}^{d-1} \exp\left(i\frac{2\pi}{d}jw\right) |j\rangle. \quad (12)$$

The measured photon coincidence counts are shown in Fig. 3(b). Genuine  $d$ -dimensional entanglement can be confirmed if the calculated state fidelity  $F_d > B_{d-1} = (d - 1)/d$  [44]. From the measurements in the constructed MUB, we obtain a fidelity  $F_3$  of  $71.57 \pm 1.39\%$ , which is above the bound of  $B_2 = 2/3 \approx 66.7\%$ . Thus, we certify the existence of genuine three-dimensional OAM entanglement in our experiment.

#### IV. CONCLUSIONS

In conclusion, we have experimentally generated a high-dimensional hyperentangled state from two parallel SFWM processes with BD interferometers. The results of concurrence and purity confirm the presence of both path entanglement and two-dimensional OAM entanglement. In addition, three-dimensional OAM entanglement is confirmed by Bell-type inequalities and fidelity. Due to the reason that the path has infinite dimensions theoretically like OAM, the path is a potential degree of freedom to apply to future quantum technologies and fundamental tests as a source of high-dimensional entanglement [46,47]. Hyperentanglement has been realized as a promising resource to significantly increase channel capacity, improve robustness, and provide better security [48]. By introducing high-dimensional hyperentanglement, our system will directly reduce the attack probability for the eavesdropper, which is smaller than that of the schemes using two-dimensional entangled states as quantum channels

[49]. Since our system has already found many applications in the CV region, such as quantum images [34,35], tunable delay of entanglement [50], heralded generation of single photons [36], and large-scale quantum networks [29,30], our results here pave the way for exploring DV-CV hybrid quantum systems [37–39] from a warm atomic ensemble.

#### ACKNOWLEDGMENTS

This work was funded by Innovation Program of Shanghai Municipal Education Commission (Grant No. 2021-01-07-00-08-E00100), National Natural Science

Foundation of China (Grants No. 11874155, No. 91436211, No. 11374104, and No. 12174110), Basic Research Project of Shanghai Science and Technology Commission (Grant No. 20JC1416100), Natural Science Foundation of Shanghai (Grant No. 17ZR1442900), Minhong Leading Talents (Grant No. 201971), Shanghai Municipal Science and Technology Major Project (Grant No. 2019SHZDZX01), and the 111 project (Grant No. B12024). Shanghai Sailing Program (Grant No. 21YF1410800)

Q.H. and Y.R. contributed equally to this work.

- 
- [1] L. Duan, M. D. Lukin, J. I. Cirac, and P. Zoller, Long-distance quantum communication with atomic ensembles and linear optics, *Nature (London)* **414**, 413 (2001).
- [2] K. Edamatsu, R. Shimizu, and T. Itoh, Measurement of the Photonic de Broglie Wavelength of Entangled Photon Pairs Generated by Spontaneous Parametric Down-Conversion, *Phys. Rev. Lett.* **89**, 213601 (2002).
- [3] M. W. Mitchell, J. S. Lundeen, and A. M. Steinberg, Super-resolving phase measurements with a multiphoton entangled state, *Nature (London)* **429**, 161 (2004).
- [4] Y. S. Kim, O. Kwon, S. M. Lee, J. C. Lee, H. Kim, S. K. Choi, H. S. Park, and Y. H. Kim, Observation of Young's double-slit interference with the three-photon N00N state, *Opt. Express* **19**, 24957 (2011).
- [5] Y. Guo, X.-M. Hu, B.-H. Liu, Y.-F. Huang, C.-F. Li, and G.-C. Guo, Experimental realization of path-polarization hybrid high-dimensional pure state, *Opt. Express* **26**, 28918 (2018).
- [6] P. G. Kwiat, K. Mattle, H. Weinfurter, A. Zeilinger, A. V. Sergienko, and Y. Shih, New High-Intensity Source of Polarization-Entangled Photon Pairs, *Phys. Rev. Lett.* **75**, 4337 (1995).
- [7] J. Park, H. Kim, and H. S. Moon, Polarization-Entangled Photons from a Warm Atomic Ensemble Using a Sagnac Interferometer, *Phys. Rev. Lett.* **122**, 143601 (2019).
- [8] M. Kues, C. Reimer, P. Roztocki, L. R. Cortés, S. Sciara, B. Wetzell, Y. Zhang, A. Cino, S. T. Chu, B. E. Little, D. J. Moss, L. Caspani, J. Azaña, and R. Morandotti, On-chip generation of high-dimensional entangled quantum states and their coherent control, *Nature (London)* **546**, 622 (2017).
- [9] E. Bimbard, N. Jain, A. MacRae, and A. Lvovsky, Quantum-optical state engineering up to the two-photon level, *Nat. Photonics* **4**, 243 (2010).
- [10] A. Mair, A. Vaziri, G. Weihs, and A. Zeilinger, Entanglement of the orbital angular momentum states of photons, *Nature (London)* **412**, 313 (2001).
- [11] A. Vaziri, G. Weihs, and A. Zeilinger, Experimental Two-Photon, Three-Dimensional Entanglement for Quantum Communication, *Phys. Rev. Lett.* **89**, 240401 (2002).
- [12] W. Zhang, D.-S. Ding, M.-X. Dong, S. Shi, K. Wang, S.-L. Liu, Y. Li, Z.-Yuan Zhou, B.-S. Shi and G.-C. Guo, Experimental realization of entanglement in multiple degrees of freedom between two quantum memories, *Nat. Commun.* **7**, 13514 (2016).
- [13] X. M. Hu, W. B. Xing, B. H. Liu, D. Y. He, H. Cao, Y. Guo, C. Zhang, H. Zhang, Y. F. Huang, C. F. Li, and G. C. Guo, Efficient distribution of high-dimensional entanglement through 11 km fiber, *Optica* **7**, 738 (2020).
- [14] A. C. Dada, J. Leach, G. S. Buller, M. J. Padgett, and E. Andersson, Experimental high-dimensional two-photon entanglement and violations of generalized Bell inequalities, *Nat. Phys.* **7**, 677 (2011).
- [15] C. Schaeff, R. Polster, M. Huber, S. Ramelow, and A. Zeilinger, Experimental access to higher-dimensional entangled quantum systems using integrated optics, *Optica* **2**, 523 (2015).
- [16] P. G. Kwiat, Hyper-entangled states *J. Mod. Opt.* **44**, 2173 (1997).
- [17] T. M. Zhao, Y. S. Ihn, and Y. H. Kim, Direct Generation of Narrow-Band Hyperentangled Photons, *Phys. Rev. Lett.* **122**, 123607 (2019).
- [18] Z. D. Xie, T. Zhong, S. Shrestha, X. A. Xu, J. L. Liang, Y. X. Gong, J. C. Bienfang, A. Restelli, J. H. Shapiro, F. N. C. Wong and C. W. Wong, Harnessing high-dimensional hyperentanglement through a biphoton frequency comb, *Nat. Photonics* **9**, 536 (2015).
- [19] S. M. Lee, H. Kim, M. Cha, and H. S. Moon, Polarization-entangled photon-pair source obtained via type-II non-collinear SPDC process with PPKTP crystal, *Opt. Express* **24**, 2941 (2016).
- [20] K. Liao, H. Yan, J. He, S. Du, Z. M. Zhang, and S. L. Zhu, Subnatural-Linewidth Polarization-Entangled Photon Pairs with Controllable Temporal Length, *Phys. Rev. Lett.* **112**, 243602 (2014).
- [21] H. Yan, S. Zhang, J. F. Chen, M. M. T. Loy, G. K. L. Wong, and S. Du, Generation of Narrow-Band Hyperentangled Nondegenerate Paired Photons, *Phys. Rev. Lett.* **106**, 033601 (2011).
- [22] P. Chen, X. Guo, C. Shu, M. M. T. Loy, and S. Du, Frequency-induced phase-tunable polarization-entangled narrowband biphotons, *Optica* **2**, 505 (2015).
- [23] C. Shu, P. Chen, T. K. A. Chow, L. B. Zhu, Y. H. Xiao, M. M. T. Loy and S. W. Du, Subnatural-linewidth biphotons from a Doppler-broadened hot atomic vapour cell, *Nat. Commun.* **7**, 12783 (2016).
- [24] J. Park, T. Jeong, H. Kim, and H. S. Moon, Time-Energy Entangled Photon Pairs from Doppler-Broadened Atomic Ensemble via Collective Two-Photon Coherence, *Phys. Rev. Lett.* **121**, 263601 (2018).
- [25] Q. F. Chen, B. S. Shi, Y. S. Zhang, and G. C. Guo, Entanglement of the orbital angular momentum states of the photon pairs

- generated in a hot atomic ensemble, *Phys. Rev. A* **78**, 053810 (2008).
- [26] S. Shi, M. X. Dong, Y. C. Yu, Y. H. Ye, W. Zhang, K. Wang, G. C. Guo, D. S. Ding, and B. S. Shi, Entangled qutrits generated in four-wave mixing without post-selection, *Opt. Express* **28**, 11538 (2020).
- [27] X. Pan, S. Yu, Y. Zhou, K. Zhang, K. Zhang, S. Lv, S. Li, W. Wang, and J. Jing, Orbital-Angular-Momentum Multiplexed Continuous-Variable Entanglement from Four-Wave Mixing in Hot Atomic Vapor, *Phys. Rev. Lett.* **123**, 070506 (2019).
- [28] S. Li, X. Pan, Y. Ren, H. Liu, S. Yu, and J. Jing, Deterministic Generation of Orbital-Angular-Momentum Multiplexed Tripartite Entanglement, *Phys. Rev. Lett.* **124**, 083605 (2020).
- [29] K. Zhang, W. Wang, S. Liu, X. Pan, J. Du, Y. Lou, S. Yu, S. Lv, N. Treps, C. Fabre, and J. Jing, Reconfigurable Hexapartite Entanglement by Spatially Multiplexed Four-Wave Mixing Processes, *Phys. Rev. Lett.* **124**, 090501 (2020).
- [30] W. Wang, K. Zhang, and J. Jing, Large-Scale Quantum Network over 66 Orbital Angular Momentum Optical Modes, *Phys. Rev. Lett.* **125**, 140501 (2020).
- [31] S. Liu, Y. Lou and J. Jing, Orbital angular momentum multiplexed deterministic all-optical quantum teleportation, *Nat. Commun.* **11**, 3875 (2020).
- [32] O. J. Fariás, G. H. Aguilar, A. Valdés-Hernández, P. H. Souto Ribeiro, L. Davidovich, and S. P. Walborn, Observation of the Emergence of Multipartite Entanglement Between a Bipartite System and its Environment, *Phys. Rev. Lett.* **109**, 150403 (2012).
- [33] Y.-H. Kim, R. Yu, S. P. Kulik, Y. Shih, and M. O. Scully, Delayed “Choice” Quantum Eraser, *Phys. Rev. Lett.* **84**, 1 (2000).
- [34] V. Boyer, A. M. Marino, R. C. Pooser, and P. D. Lett, Entangled images from four-wave mixing, *Science* **321**, 544 (2008).
- [35] V. Boyer, A. M. Marino, and P. D. Lett, Generation of Spatially Broadband Twin Beams for Quantum Imaging, *Phys. Rev. Lett.* **100**, 143601 (2008).
- [36] A. MacRae, T. Brannan, R. Achal, and A. I. Lvovsky, Tomography of a High-Purity Narrowband Photon from a Transient Atomic Collective Excitation, *Phys. Rev. Lett.* **109**, 033601 (2012).
- [37] U. L. Andersen, J. S. N. Nielsen, P. van Loock, and A. Furusawa, Hybrid discrete- and continuous-variable quantum information, *Nat. Phys.* **11**, 713 (2015).
- [38] A. Zavatta, S. Viciani, and M. Bellini, Quantum-to-classical transition with single-photon-added coherent states of light, *Science* **306**, 660 (2004).
- [39] O. Morin, K. Huang, J. L. Liu, H. L. Jeannic, C. Fabre, and J. Laurat, Remote creation of hybrid entanglement between particle-like and wave-like optical qubits, *Nat. Photonics* **8**, 570 (2014).
- [40] S. P. Walborn, A. N. de Oliveira, R. S. Thebaldi, and C. H. Monken, Entanglement and conservation of orbital angular momentum in spontaneous parametric down-conversion, *Phys. Rev. A* **69**, 023811 (2004).
- [41] D. F. V. James, P. G. Kwiat, W. J. Munro, and A. G. White, Measurement of qubits, *Phys. Rev. A* **64**, 052312 (2001).
- [42] J. B. Altepeter, E. R. Jeffrey, and P. G. Kwiat, Photonic state tomography, photonic state tomography, *Adv. At. Mol. Opt. Phys.* **52**, 105 (2005).
- [43] D. Collins, N. Gisin, N. Linden, S. Massar, and S. Popescu, Bell Inequalities for Arbitrarily High-Dimensional Systems, *Phys. Rev. Lett.* **88**, 040404 (2002).
- [44] J. Bavaresco, N. Herrera Valencia, C. Klöckl, M. Pivoluska, P. Erker, N. Friis, M. Malik and M. Huber, Measurements in two bases are sufficient for certifying high-dimensional entanglement, *Nat. Phys.* **14**, 1032 (2018).
- [45] W. K. Wootters and B. D. Fields, Optimal state-determination by mutually unbiased measurements, *Ann. Phys.* **191**, 363 (1989).
- [46] J. Kysela, M. Erhard, A. Hochrainer, M. Krenn, and A. Zeilinger, Path Identity as a Source of High-Dimensional Entanglement, *Proc. Natl. Acad. Sci. USA* **117**, 26118 (2020).
- [47] X.-M. Hu, W.-B. Xing, B.-H. Liu, Y.-F. Huang, C.-F. Li, G.-C. Guo, P. Erker, and M. Huber, Efficient Generation of High-Dimensional Entanglement Through Multipath Down-Conversion, *Phys. Rev. Lett.* **125**, 090503 (2020).
- [48] F.-G. Deng, B.-C. Ren, and X.-H. Li, Quantum hyperentanglement and its applications in quantum information processing, *Sci. Bull.* **62**, 46 (2017).
- [49] J. Shi, Y.-X. Gong, P. Xu, S.-N. Zhu, and Y.-B. Zhan, Quantum secure direct communication by using three-dimensional hyperentanglement, *Commun. Theor. Phys.* **56**, 831 (2011).
- [50] A. M. Marino, R. C. Pooser, V. Boyer and P. D. Lett, Tunable delay of Einstein-Podolsky-Rosen entanglement, *Nature (London)* **457**, 859 (2009).